

Topographical and electrochemical nanoscale imaging of living cells using voltage-switching mode scanning electrochemical microscopy

Yasufumi Takahashi^{a,1}, Andrew I. Shevchuk^b, Pavel Novak^c, Babak Babakinejad^c, Julie Macpherson^d, Patrick R. Unwin^d, Hitoshi Shiku^e, Julia Gorelik^f, David Klennerman^g, Yuri E. Korchev^{c,1}, and Tomokazu Matsue^{a,e,1}

^aWorld Premier International Research Center-Advanced Institute for Materials Research, Tohoku University, Katahira, Aoba 2-1-1, Sendai 980-8577, Japan; ^bInstitute for Life Sciences, University of Southampton, 3046, Highfield Campus, Southampton SO17 1BJ, United Kingdom; ^cDivision of Medicine, Imperial College London, Hammersmith Hospital Campus, London W12 0NN, United Kingdom; ^dDepartment of Chemistry, University of Warwick, Coventry CV4 7AL, West Midlands, United Kingdom; ^eGraduate School of Environmental Studies, Tohoku University, Aramaki Aoba 6-6-11-605, Sendai 980-8579, Japan; ^fNational Heart and Lung Institute, Department of Heart Science, Imperial College London, Hammersmith Hospital Campus, London W12 0NN, United Kingdom; and ^gDepartment of Chemistry, Cambridge University, Cambridge CB2 1EW, United Kingdom

Edited by Royce W. Murray, University of North Carolina, Chapel Hill, NC, and approved April 11, 2012 (received for review February 29, 2012)

We describe voltage-switching mode scanning electrochemical microscopy (VSM-SECM), in which a single SECM tip electrode was used to acquire high-quality topographical and electrochemical images of living cells simultaneously. This was achieved by switching the applied voltage so as to change the faradaic current from a hindered diffusion feedback signal (for distance control and topographical imaging) to the electrochemical flux measurement of interest. This imaging method is robust, and a single nanoscale SECM electrode, which is simple to produce, is used for both topography and activity measurements. In order to minimize the delay at voltage switching, we used pyrolytic carbon nanoelectrodes with 6.5–100 nm radii that rapidly reached a steady-state current, typically in less than 20 ms for the largest electrodes and faster for smaller electrodes. In addition, these carbon nanoelectrodes are suitable for convoluted cell topography imaging because the RG value (ratio of overall probe diameter to active electrode diameter) is typically in the range of 1.5–3.0. We first evaluated the resolution of constant-current mode topography imaging using carbon nanoelectrodes. Next, we performed VSM-SECM measurements to visualize membrane proteins on A431 cells and to detect neurotransmitters from a PC12 cells. We also combined VSM-SECM with surface confocal microscopy to allow simultaneous fluorescence and topographical imaging. VSM-SECM opens up new opportunities in nanoscale chemical mapping at interfaces, and should find wide application in the physical and biological sciences.

high-resolution imaging | living cell imaging | noninvasive | constant-distance mode

Scanning electrochemical microscopy (SECM) uses an electrode tip for detecting electroactive chemical species and is an effective tool for the investigation of the localized chemical properties of sample surfaces and interfaces (1). Because SECM has high temporal resolution and can be used under physiological conditions, it is particularly well suited for quantitative measurements of (short-lived) chemicals like neurotransmitters, nitric oxide, reactive oxygen species, and oxygen, which are released/consumed by living cells. In conventional SECM, the probe is often micrometer scale and the probe vertical position is kept at a constant height, a plane, during probe scanning. If the sample topography is not flat, the electrode-sample separation changes during scanning, complicating the SECM measurement and its analysis.

Various methods for SECM electrode miniaturization and control of the electrode-sample separation have been advocated in order to improve the resolution of SECM imaging. The reliable fabrication of nanoelectrodes with a small ratio of electrode-insulation to active electrode (RG) is of particular importance to improve SECM spatial resolution (2). In particular, a variety

of different approaches have been adopted to create small electrodes with thin insulating coats such as photolithography (3), chemical vapor deposition (4), electrodeposited paint methods (5, 6), laser pulling techniques (7–11), and pyrolytic carbon deposition (12–15). Photolithography and chemical vapor deposition can be used to make thin insulation layers, but pinholes are often a problem. The laser pulling technique is effective and reproducible, but this method requires special polishing techniques or focused ion beam milling to expose the metal region. On the other hand, pyrolytic carbon deposition inside glass pipettes enables fabrication of nano-sized electrodes with insulation of excellent integrity. This type of electrode has proven powerful for living cell measurements (14, 15), and we thus use it for the studies herein.

Control of the electrode-sample distance is also critical for electrochemical measurements free from topographical artifacts but has proved difficult to achieve to date. AFM (4, 5, 16), shear force (3, 17–19), impedance (14, 20–22), faradaic current (7, 14, 23), ion current (6, 15, 24), and electrochemical (25–27) feedback distance-control systems have been developed, but many of these required additional probe modifications for distance control. Impedance-feedback and constant-current distance control are effective methods to obtain high-resolution topography images because they do not require additional modification of the electrode for distance control. However, the impedance-feedback mode has resolution limitations due to the principle of the measurement (14). The constant-current mode has been shown to be capable of high-resolution imaging, but only for topography hitherto (7, 23).

Here, we report a voltage-switching mode (VSM)-SECM, developed to achieve constant-distance mode measurements and the possibility of (electro)chemical flux measurements at the same location. Full details of the protocol for VSM-SECM and the probe fabrication method are given in the experimental section. In brief, the imaging protocol involved first translating the tip electrode toward the surface while detecting the distance-dependent current for the hindered diffusion of a redox-active solute to the tip [reduction of either $\text{Ru}(\text{NH}_3)_6^{3+}$ or oxygen for the studies herein], with the probe potential biased to carry out

Author contributions: Y.T., H.S., Y.E.K., and T.M. designed research; Y.T., A.I.S., and B.B. performed research; Y.T., A.I.S., P.N., B.B., J.G., D.K., Y.E.K., and T.M. contributed new reagents/analytic tools; Y.T., J.M., P.R.U., Y.E.K., and T.M. analyzed data; and Y.T., A.I.S., P.N., J.M., P.R.U., H.S., J.G., D.K., Y.E.K., and T.M. wrote the paper.

The authors declare no conflict of interest.

This article is a PNAS Direct Submission.

¹To whom correspondence may be addressed. E-mail: takahashi@bioinfo.che.tohoku.ac.jp, y.korchev@imperial.ac.uk, or matsue@bioinfo.che.tohoku.ac.jp.

This article contains supporting information online at www.pnas.org/lookup/suppl/doi:10.1073/pnas.1203570109/-DCSupplemental.

the cathodic process. When the current diminished compared to bulk solution by a set amount, this indicated that the probe was at a desired distance from the surface or structure of interest (typically one electrode radius away). The motion of the probe was arrested and the z -position of the piezoelectric position was registered. By carrying out this process at a number of points over the surface, the topography was mapped out. Additionally, for concomitant flux measurements, when the electrode reached the desired position from the surface, at each tip approach, the applied voltage could be switched positive to permit electrochemical (flux) imaging of the sample surface.

Pyrolytic carbon nanoelectrodes (generally 6.5–100 nm radius, but occasionally larger, *vide infra*) were used to obtain high-resolution topographical and electrochemical images. The nanoelectrode reaches a steady-state current very quickly when switching the voltage applied to the nanoelectrode, because the time scale for both double-layer charging and the establishment of steady-state diffusion scale with the electrode dimension (28, 29). Another advantage of this measurement, as we highlight herein, is that it does not require additional modification of a simple tip electrode to achieve distance control. More generally, a key advantage of this approach, compared to fluorescence-based methods for functional imaging, is that chemical fluxes and concentrations of target species can be determined at a local electrode on a fast time scale, without the need for fluorescence labels, which tends to limit the range of detectable species and may also interfere with the living system.

To demonstrate the efficacy of VSM-SECM, we performed imaging of membrane proteins on A431 cells and the detection of neurotransmitters from neurons. Furthermore, we combined constant-current SECM in hopping mode and confocal microscopy for simultaneous topographical and fluorescence measurements. This combined approach served to illustrate the additional information that could be obtained on the biological structures, compared to conventional fluorescence-based methods.

Results

Characterization of the Carbon Electrodes. The topographical resolution in the SECM constant-current mode depends on the size and aspect ratio of the electrode. In this report, we used carbon nanoelectrodes produced by the pyrolytic decomposition of butane gas. The details of the fabrication method are described in the experimental section. Fig. 1A shows field emission-scanning electron microscope (FE-SEM) images of a carbon nanoelectrode.

lectrode produced for these studies. The nanoelectrode is quite sharp (cone angle of the tip is 10), and the radii of the carbon and outer glass were 22 nm and 65 nm, respectively. However, the deposited carbon region is difficult to recognize even when using FE-SEM, and we therefore routinely characterized electrodes using approach curve recordings (Fig. 1B). Probes radii were estimated from steady-state currents in bulk solution, i_d assuming disk type electrodes with an RG (glass radius to electrode radius) value of 1.5,

$$i_d = 4.64nFC^*Da,$$

where n is the number of electrons transferred in the tip reaction, F is the faraday constant, $D = 6.5 \times 10^{-6} \text{ cm}^2 \text{ s}^{-1}$ is the diffusion coefficient of FcCH_2OH , of concentration C^* in solution. These calculated tip radii (150 nm and 6.4 nm for the data shown in Fig. 1B) were used to produce theoretical approach curves for the same tip geometric parameters. The current profiles were fitted to established theoretical curves for a simple disk geometry (30–32). Good correlation was observed between theory and experiment. Therefore, the pyrolytic carbon nanoelectrode is effectively planar and can be used for high-resolution electrochemical microscopy imaging and quantitative analysis of electrochemical species.

Constant-Current Mode Topographical Imaging. Hydrophilic redox mediators are useful for living cell topography imaging because they cannot cross the cell membrane, and so the diffusion-limited faradaic current for such a species in the bulk solution decreases with the SECM tip electrode to (cell membrane) surface in a defined manner (2). This is well illustrated, for example, by the studies of Baur and coworkers who imaged cell topography by both constant-height mode and constant-distance mode SECM using hydrophilic mediators (14, 33). A variety of electrochemical mediators were assessed for toxicity to living cell and $\text{Ru}(\text{NH}_3)_6^{3+}$ was selected as a suitable mediator. Constant-current mode SECM is a particularly interesting means of noncontact topography imaging because the working distance of the tip that records the feedback signal is large compared with an imaging technique such as AFM. This ensures ready access of nutrients, metabolites, and waste products to and from the cell. On the other hand, structures with steep slope regions, small protrusions, or wave structures can be considered potentially challenging to image with constant-current (hindered diffusion) feedback SECM (2), because the spatial resolution is convoluted to some extent by the overall probe size. A small RG electrode with a small active radius electrode is needed to achieve the best spatial resolution. As highlighted above, it was for these reasons that we fabricated carbon nanoelectrodes with small RG to meet the requirements for high-resolution imaging. The topographical measurements were typically performed in phosphate buffered saline (PBS) containing 10 mM $\text{Ru}(\text{NH}_3)_6\text{Cl}_3$. To illustrate the applicability of constant-current mode topography imaging with our probes, we imaged boar spermatozoon, differentiated rat adrenal pheochromocytoma cells (PC12), A431 cells, cardiac myocytes, and auditory hair cells.

Fig. 2 shows a typical set of topography images. For the boar spermatozoon and PC12 cells, the boundary area between the cell and the substrate surface is such that there is a steep slope in the topography, which would difficult to image faithfully with conventional scanning probe microscope methods. Evidently, the hopping-mode scanning algorithm (defined briefly above; also see *Materials and Methods*) is able to visualize the structures clearly. Indeed, the topographical features of boar spermatozoon and PC12 revealed by SECM are very similar to those previously obtained with SICM (15, 34), which is regarded highly as an ultrahigh-resolution in situ imaging technique. Further evidence for the powerful nature of the SECM technique comes from the

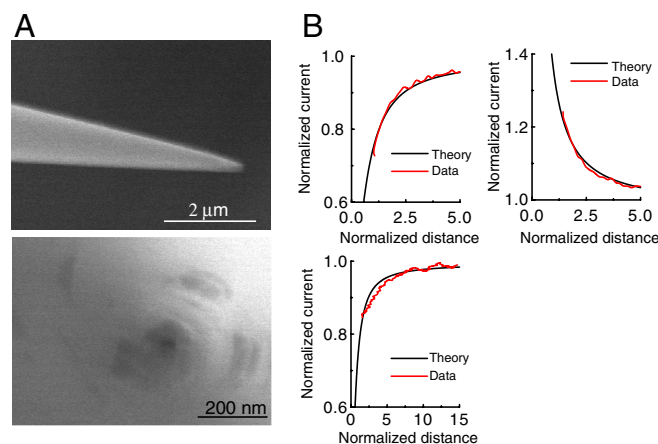


Fig. 1. (A) FE-SEM images of side and top view of the carbon nanoelectrode. (B) Approach curves in a 1.0 mM FcCH_2OH (diffusion-limited oxidation) and PBS for electrochemical measurements on insulating (Left) and unbiased conducting (Right) substrate. The electrode was held at 500 mV vs. Ag/AgCl . The RG values of the theoretical curves were estimated to be 1.5. The radii of the carbon electrodes estimated from steady-state current were 150 nm (Top) and 6.4 nm (Bottom), respectively.

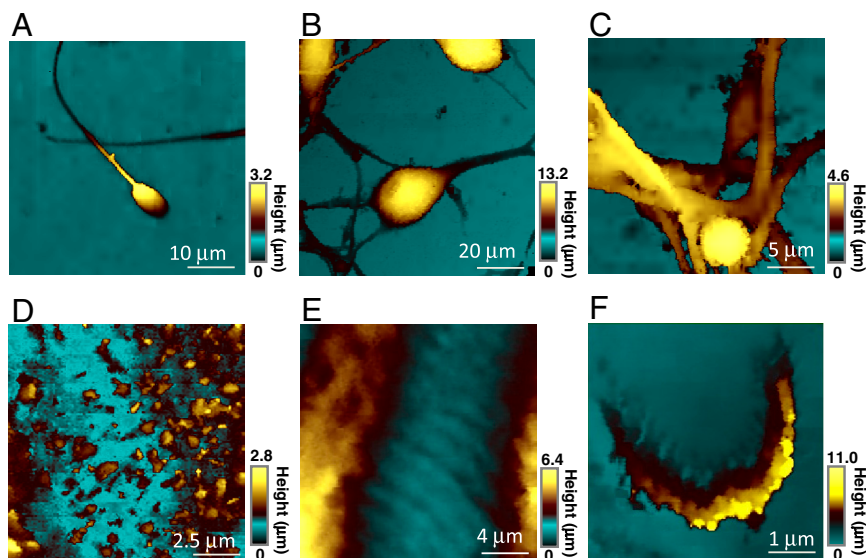


Fig. 2. Constant-current topography images of (A) boar sperm cell, (B and C) differentiated PC12, (D) A431 cell, (E) cardiac myocyte, and (F) hair cells. The carbon electrode was held at -500 mV vs. Ag/AgCl in PBS containing 10 mM $\text{Ru}(\text{NH}_3)_6\text{Cl}_3$ [diffusion-limited reduction of $\text{Ru}(\text{NH}_3)_6^{3+}$]. The electrode radii are (A) 395.1 nm, (B and C) 18.9 nm, (D) 61.8 nm, (E) 12.0 nm, (F) 70.4 nm, respectively.

fact that the neurite and varicosity, which administrate neuron transduction and axon formation, of PC12 cells were visualized much more clearly compared with a previous SECM report using more conventional imaging protocols (14).

In A431 cells and cardiac myocyte topography imaging, very sharp (small RG) electrodes were required to visualize the small protrusions or wave structures. By using carbon nanoelectrode with RG 3.0 ($a = 12$ nm), both the microvilli (0.6 – 0.8 μm in width and 0.8 – 1.0 μm in height) and sarcolemma structure (1.5 – 2.0 μm in width and 200 – 300 nm in height) were visualized clearly. Despite many studies of cells with SECM (9, 35), these SECM images reveal clearly the microstructure on living cell surfaces, representing a significant advance for SECM topography imaging. Topography measurements with scanned probe microscopy are most challenging for auditory hair cells because of features with high aspect ratio (36). With the method herein, we were able to visualize individual 250 nm in height stereocilia structure. All the images clearly show cell features without artifacts. These results thus indicate that very high-quality images of cellular topography can be obtained using (hindered diffusion) constant-current hopping-mode SECM in conjunction with carbon nanoelectrodes.

Simultaneous Electrochemical and Topographical Imaging in Voltage-Switching Mode. We further improved the system to conduct high-resolution electrochemistry and topography imaging of living cells with a single electrode probe. To achieve this, a voltage-switching protocol was adopted. Highly reliable distance control was achieved using the constant-current hopping mode with $\text{Ru}(\text{NH}_3)_6^{3+}$ reduction to give topographic images, as described above, while electrochemical measurements at the same tip electrode were recorded in a different potential region, with the tip at a defined (known) distance from the surface of interest. SECM experiments have been reported previously using one mediator to record topography and one to obtain tissue permeability (activity) (37), but the studies herein are a great advance because the imaging is simultaneous, has topographical feedback, and is nanoscale.

We applied VSM-SECM to image epidermal growth factor receptor (EGFR), which is one of the key membrane proteins associated with cancer, on cell surfaces (38). Epidermal growth factor (EGF) binds to the EGFR, and the activated EGFR initiates the signaling cascades, thereby promoting cell proliferation,

differentiation, apoptosis, and migration. The evaluation of EGFR expression levels on cell surfaces is thus important but extremely difficult to achieve. In previous work, we evaluated EGFR expression level using SECM (39, 40), but it was impossible to identify a cell with high EGFR expression from others when the cells were in a confluent stage. The limitation arose because images had to be taken with a relatively large electrode in conventional constant-height mode. In the present study, we used a 650 -nm radius carbon electrode for VSM-SECM in Hepes buffer containing 4.7 mM *p*-aminophenyl phosphate (PAPP). EGFR was labeled with alkaline phosphatase (ALP)-tagged antibody. The ALP-catalyzed reaction produces *p*-aminophenol (PAP), which can be detected by oxidation, giving an electrochemical signal, which indicates the presence of EGFR on the cell surface. Fig. 3*A* illustrates the timing of the VSM measurement. The electrode was set at -0.5 V vs. Ag/AgCl to detect the diffusion-limited reduction current of $\text{Ru}(\text{NH}_3)_6^{3+}$ for distance control. When the electrode approached the set point the applied voltage was switched to $+0.35$ V vs. Ag/AgCl quasi-reference electrode to achieve oxidation of PAP. In this measurement, an electrode with a 650 -nm radius was used and the ALP activity was monitored at 800 nm electrode-sample distance.

Fig. 3*B* shows the topography and electrochemical images of A431 cells. The VSM yields highly resolved topographical structures and electrochemical fields. From the images, it is evident that EGFR is not evenly distributed on the cell surfaces; also EGFR distribution is not directly correlated with the microvilli and lamellipodium, which are clearly seen in the topography image. This result demonstrates that the VSM-SECM is potentially promising for nanoscale chemical mapping at biological interfaces.

Neurotransmitter Detection Using Faradaic Current Feedback. Next, we combined the sample height information obtained by constant-current mode SECM combined with fluorescence microscopy so that we could perform measurements at the specific fluorophore-labeled structures on a cell, in this case at the synapse of neuron. Previously, a hybrid SICM-confocal system was developed based on a similar concept (41, 42), and we used a similar system in which the SECM scanner was integrated on an inverted confocal microscope. For the fluorescence measurement, the hippocampal neurons were stained with FM 1–43, which labeled synaptic vesicles (36). The measurement was performed in buffer solution with 10 mM $\text{Ru}(\text{NH}_3)_6\text{Cl}_3$ added.

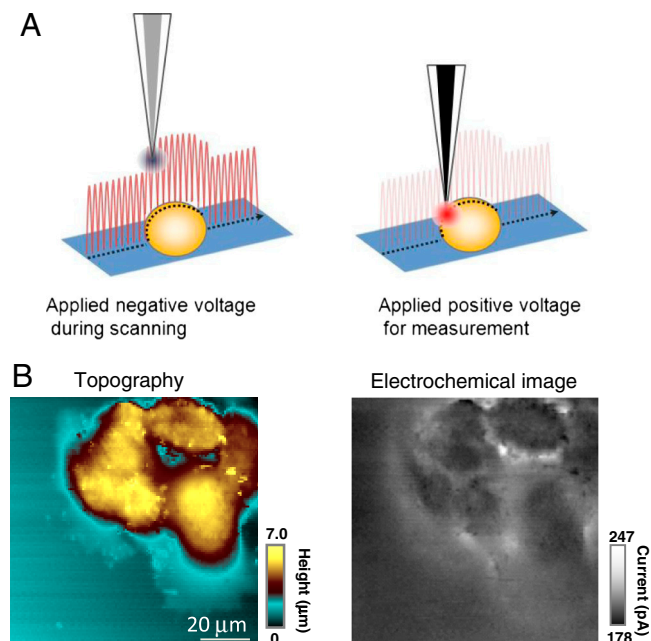


Fig. 3. (A) Schematic illustration of voltage-switching mode SECM, in which a signal for the hindered diffusion of a mediator is implemented in hopping mode (probe approach at each pixel) to trace the topography of the surface (Left) and at each set point (closest distance) an interfacial flux measurement (electrochemical activity) is made after switching the voltage (Right). (B) Topography (Left) and electrochemical (Right) images of A431 cells. The carbon electrode was held at -500 mV (topography) and 350 mV (electrochemical activity) vs. Ag/AgCl in Hepes buffer containing 10 mM $\text{Ru}(\text{NH}_3)_6\text{Cl}_3$ and 4.7 mM PAPP. The electrode radius is 721.5 nm.

Simultaneously acquired images of the topography of hippocampus neurons from SECM and the fluorescence signal of stained synaptic vesicles are shown in Fig. 4A. Fluorescence signals are observed on the varicosity, and the corresponding SECM topographical image clearly shows that these represent synaptic boutons, with heights of 4 – 6 μm .

Next, we measured neurotransmitter release from single PC12 cells. The measurements were performed in Hepes-based saline solution (10 mM Hepes, 150 mM NaCl, 4.2 mM KCl, and 11.2 mM glucose; pH 7.4). In this experiment, we used relatively large electrodes ($a = 6.0$ μm) to detect neurotransmitter effectively, based on the rationale outlined in earlier work for both NO and neurotransmitter detection (43–48). The carbon electrode was simply aligned optically over the cell and positioned one radius above the cell surface using the reduction current at a potential of -1.0 V, due to oxygen reduction, which was found to provide reliable distance control. The set point was 75% of I_{ss} . After electrode-cell distance control, the voltage applied to the carbon electrode was switched to $+0.65$ V vs. reference Ag/AgCl electrode in order to detect neurotransmitters as a function of time via the current response. Note that in this case we made a measurement in this one position over a long time period. To stimulate neurotransmitter release, we depolarized a PC12 cell by stimulation of the whole cell with 105 mM K^+ by using another micropipette (3 μm diameter). To enhance the sensitivity of the electrochemical detection, we fabricated a conically shaped carbon electrode by depositing additional carbon on the outside of the pipette as previously described (15). The steady-state current measured in 1.0 mM FcCH_2OH and PBS was 2.0 nA, corresponding to an effective electrode radius of 6.0 μm . Fig. 4B shows a series of current spikes corresponding to the release of the neurotransmitter, which was detected by the pyrolytic carbon electrode. The insets of Fig. 4B show expanded

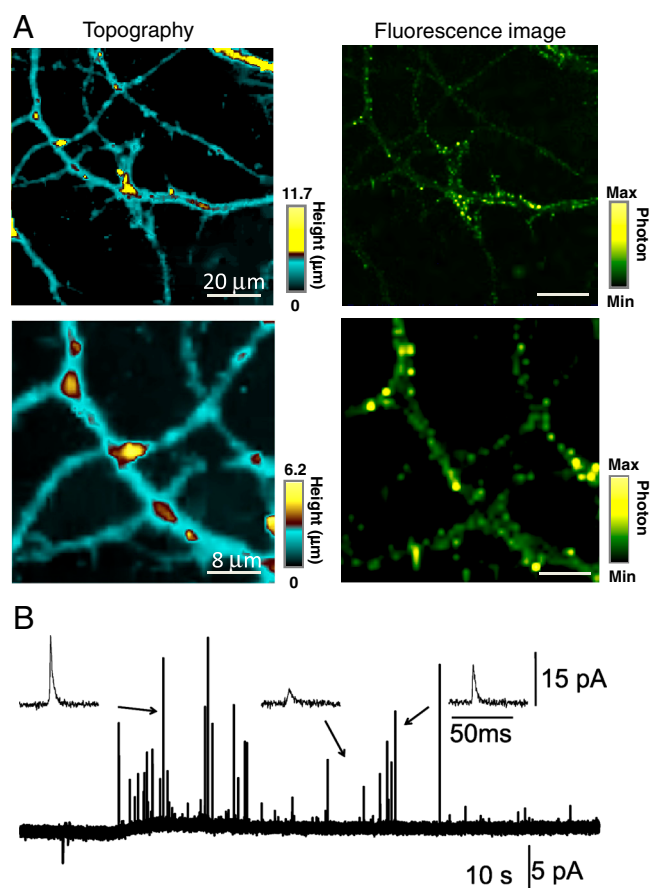


Fig. 4. (A) Topography (Left) and fluorescence (Right) images of hippocampus neurons using constant-current mode SECM combined with confocal microscopy. The carbon electrode was held at -500 mV vs. Ag/AgCl in PBS containing 10 mM $\text{Ru}(\text{NH}_3)_6\text{Cl}_3$. The electrode radius is 32.6 nm. (B) Detection of the release of the neurotransmitter using a conical-shaped carbon nanoelectrode (described in the text). A series of current spikes corresponding to neurotransmitter release detected after whole cell stimulation of 105 mM K^+ using another micropipette. The carbon electrode was held at 650 mV vs. Ag/AgCl electrode. The electrode radius is 6.0 μm .

views of the released neurotransmitter, where the amplitudes and the widths of the spike are clearly visible. It was shown previously that the amplitude and shape of the signal depends on the separation between the electrode and release site (49). Because the distance between the probe and the neuron is known with our positioning protocol, we envisage that much more information could be obtained by adopting this type of tip positioning for such measurements, making them amenable to quantitative treatment. Given the considerable interest in using small-scale carbon electrode to detect events at single neurons, these data highlight considerable future possibilities of these types of probes.

Conclusions

We have demonstrated VSM-SECM as a powerful technique for simultaneous topography and electrochemical flux measurements to detect EGFR on A431 cells surface and neurotransmitter release from a PC12 cell. Furthermore, we have shown that VSM-SECM has the potential to be combined with fluorescence imaging to make measurements at defined region of the cell. The method is reliable and does not require special modification of the electrode for distance control. Moreover, because the topography and activity are determined with a single probe, simultaneously obtained images are collocated.

The very sharp and small RG carbon nanoelectrodes used in this work are easily made and are effective for high-resolution

topography imaging using constant-current (hindered diffusion) hopping-mode SECM for distance control. The potential of these electrodes is then readily switched to allow surface flux measurements at the same spot. Among the many other possibilities in the physical and life sciences, this nanoprobe would allow the mapping of sites of neurotransmitter release, together with the possibility of detecting associated changes in the cell topography that occur during exocytosis. It is important to point out that the size of the nanoelectrode probe can be tuned for a particular application, and that it can also be made smaller than the SECM-SICM probe which we reported recently (15), so enhancing the spatial resolution. In the future, it would also be interesting to investigate long time or localized intracellular measurement using this electrode.

Materials and Methods

Materials. Ferrocenylmethanol (FcCH_2OH ; Sigma-Aldrich), hexaammineruthenium (III) chloride [$\text{Ru}(\text{NH}_3)_6\text{Cl}_3$; Sigma-Aldrich], Hank's buffered salt solution (HBSS; Invitrogen), 1- μm diameter fluorescent microbeads (Sigma-Aldrich), *p*-aminophenylphosphate monosodium salt (PAPP; LKT Laboratory Inc.) were purchased and used as received. PBS was prepared from 7.2 mM $\text{Na}_2\text{HPO}_4 \cdot 12\text{H}_2\text{O}$, 2.8 mM KH_2PO_4 , and 150 mM NaCl (pH 7.4).

Electrodes. The preparation of the pyrolytic carbon nanoelectrodes was similar to the procedures described recently (15). In brief, a quartz glass capillary (o.d. 1.2 mm, i.d. 0.9 mm; Sutter Instrument) was pulled using a CO_2 laser puller (model P-2000, Sutter Instrument) using the following parameters: Heat, 780; Fil, 3; Vel, 50; Del, 155; Pull, 120.

Butane was passed through the quartz capillary by using a Tygon tube (o.d. 2.4 mm, i.d. 0.8 mm). The taper of the pipette was inserted into another quartz capillary (o.d. 1.0 mm, i.d. 0.7 mm; Sutter Instrument), which was filled with nitrogen gas to prevent oxidation of the carbon structure formed and bending of the capillary by high temperature. This approach also protected the pipette aperture from closing through softening of the quartz pipette walls. To form a pyrolytic carbon layer inside the capillary, the pipette taper was then heated with a Bunsen burner for times ranging from 3 s. We noticed that the inner butane pressure during the carbon nanoelectrode fabrication process is a very important parameter for the successful filling of the pipet with an integral pyrolytic carbon plug. We kept the pressure at about 280 kPa.

SECM System. The SECM instrument was similar to that previously described and operated in hopping mode (36). The faradaic current was measured with a dual channel MultiClamp700B patch-clamp amplifier (Axon Instruments). The electrochemical signal was filtered using low-pass filter at 200 Hz. The data were digitized and analyzed with continuous data acquisition hardware and software (Axon Digidata 1322A, Axon Instruments). The set point was typically in the range 75–90% of the reference current, I_{REF} , which was the steady-state current measured in bulk solution. The corresponding tip/substrate distance could then be estimated by reference to theoretical approach curves for the characteristic electrode (30–32). The probe position was controlled by a XY and Z piezoelectric translation stage (Physik Instrumente, 621.2CL and 621.ZCL), using an amplifier module (Physik Instrumente, E-503.00). The system was controlled by a program written in Delphi (Borland) and Code Composer Studio (Texas Instruments) for a ScanIC controller (Ionscope).

Voltage-Switching Mode. The vertical Z positioning of the carbon nanoelectrode and the movement of the sample in the XY plane were controlled by a SICM controller (Ionscope) using an SBC6711 DSP board (Innovative Integration) at a sampling frequency of 10 kHz. A five-step procedure was used to bring the electrode to sample surface and perform the electrochemical measurement at each imaging point. First, the carbon nanoelectrode was withdrawn from its existing position either by a specified distance, typically 5.0 μm . Second, the vertical position of the probe was maintained for 15 ms,

while the nanopositioning stage moved the specimen to a new imaging point in the XY plane. During this time, a reference current I_{REF} was measured as an average of the DC current through the carbon nanoelectrode. Third, the carbon nanoelectrode was lowered at constant fall rate of 30 nm/ms while monitoring the difference in current, I , between I_{REF} and the instantaneous value of current through the carbon nanoelectrode I_{MV} . As soon as I fell below the specified value of the set point, I_s , motion of the electrode stopped and the vertical position of the carbon nanoelectrode was saved into the corresponding image pixel. Then, fourth, the applied voltage of the carbon nanoelectrode was switched from negative (hindered diffusion detection) to positive for the surface flux measurement. After a wait period, typically of 20 ms to allow a steady-state current to be achieved, the electrochemical signal associated with the desired sample surface property was measured over a period of 1 ms. After the electrochemical measurement, the fifth step was for the carbon nanoelectrode to be quickly withdrawn by a specified amplitude and the potential switched from positive to negative to acquire the steady-state current for I_{REF} , after waiting 20 ms for a steady-state to be established, and to start a new measurement cycle. I_s values ranged from 75–90% of the reference current, I_{REF} . The lateral XY positioning was controlled by conventional line scanning and adaptive scanning. The latter was described in previous work (36).

EGFR Imaging. EGFR was labeled with an ALP-labeled antibody for electrochemical detection. In the case of EGFR labeling with an ALP-labeled antibody, the cells were reacted with RPMI-1640 containing an anti-EGFR antibody (1 $\mu\text{g}/\text{mL}$) for 90 min at 37 $^{\circ}\text{C}$, followed by thorough washing with RPMI-1640. The cells were then reacted with RPMI-1640 containing an ALP-labeled secondary antibody (ALP-labeled IgG) (1 $\mu\text{g}/\text{mL}$) for 90 min at 37 $^{\circ}\text{C}$, followed by thorough washing with RPMI-1640.

The measurements were performed in a Hepes-based saline solution (10 mM Hepes, 150 mM NaCl, 4.2 mM KCl, and 11.2 mM glucose; pH 9.5) containing 4.7 mM PAPP for detecting the ALP-labeled EGFR. ALP catalyzes the hydrolysis of PAPP to yield *p*-aminophenol (PAP) as an enzymatic product, which was detected electrochemically using the microelectrode probe of SECM set at +0.30 V vs. Ag/AgCl.

Cell Culture and Isolation. Cells were maintained at 37 $^{\circ}\text{C}$ in an atmosphere of humidified air with 95% O_2 /5% CO_2 . PC12 cells were kept in a growth medium consisting of an RPMI-1640 (GIBCO) supplemented with 10% heat-inactivated horse serum (GIBCO), 5% fetal calf serum (GIBCO), 100 $\mu\text{g}/\text{mL}$ streptomycin and 100 U/mL penicillin (GIBCO). The nerve growth factor (50 ng/mL, 2.5 S; GIBCO) was added to the medium for differentiation to the neuronal PC12. A431 cells were kept in a growth medium consisting of an RPMI-1640 (GIBCO) supplemented with 10% fetal calf serum (GIBCO), 100 $\mu\text{g}/\text{mL}$ streptomycin and 100 U/mL penicillin (GIBCO). Boar spermatozoa were purchased from JSR Genetics Ltd. Auditory hair cells were kindly provided by Gregory I. Frolenkov (University of Kentucky, Lexington, KY). Cardiac myocytes from adult rats were isolated by digestion of intact perfused ventricle as previously described (50). Rat hippocampal neurons were prepared as previously described (36) and cultured on glass coverslips to allow confocal microscopy. For combined topography/fluorescent measurements, hippocampal neurons were first incubated for 90 s at room temperature in 1.5 mL of loading solution to stain synaptic boutons with FM1-43, an activity-dependent marker that is accumulated in synaptic vesicles during cycles of endo- and exocytosis, and then washed three times with a total volume of at least 10 mL of standard external solution and left for 15 min in the dark before imaging.

ACKNOWLEDGMENTS. This work was funded by a Grant-in-Aid for Scientific Research (A) (No. 22245011) from the Japan Society for the Promotion of Science (JSPS), the Engineering and Physical Sciences Research Council, and the Chemical and Biological Program of the National Measurement System of the UK Department of Business, Innovation, and Skills. Y.T. acknowledges support from JSPS Postdoctoral Fellowships for Research Abroad. P.R.U. thanks the European Research Council for support (Grant ERC-2009-AdG2471143-QUANTIF).

- Amemiya S, Bard AJ, Fan FRF, Mirkin MV, Unwin PR (2008) Scanning electrochemical microscopy. *Annu Rev Anal Chem* 1:95–131.
- Kwak J, Bard AJ (1989) Scanning electrochemical microscopy—theory of the feedback mode. *Anal Chem* 61:1221–1227.
- Lee Y, Ding ZF, Bard AJ (2002) Combined scanning electrochemical/optical microscopy with shear force and current feedback. *Anal Chem* 74:3634–3643.
- Kueng A, Kranz C, Lugstein A, Bertagnolli E, Mizaikoff B (2003) Integrated AFM-SECM in tapping mode: Simultaneous topographical and electrochemical imaging of enzyme activity. *Angew Chem Int Ed Engl* 42:3238–3240.

- Ueda A, et al. (2007) Neurite imaging of living PC12 cells with scanning electrochemical/near-field optical/atomic force microscopy. *Angew Chem Int Ed Engl* 46:8238–8241.
- Takahashi Y, et al. (2010) Simultaneous noncontact topography and electrochemical imaging by SECM/SICM featuring ion current feedback regulation. *J Am Chem Soc* 132:10118–10126.
- Laforge FO, Velmurugan J, Wang YX, Mirkin MV (2009) Nanoscale imaging of surface topography and reactivity with the scanning electrochemical microscope. *Anal Chem* 81:3143–3150.

8. Shao YH, et al. (1997) Nanometer-sized electrochemical sensors. *Anal Chem* 69:1627–1634.
9. Sun P, et al. (2008) Nanoelectrochemistry of mammalian cells. *Proc Natl Acad Sci USA* 105:443–448.
10. Mauzeroll J, Mezour MA, Morin M (2011) Fabrication and characterization of laser pulled platinum microelectrodes with controlled geometry. *Anal Chem* 83:2378–2382.
11. Nagamine K, Takahashi Y, Ino K, Shiku H, Matsue T (2011) Influence of tip size on single yeast cell imaging using scanning electrochemical microscopy. *Electroanalysis* 23:1168–1174.
12. Kim YT, Scarnulis DM, Ewing AG (1986) Carbon-ring electrodes with 1- μm tip diameter. *Anal Chem* 58:1782–1786.
13. Wong DKY, Xu LYF (1995) Voltammetric studies of carbon disk electrodes with submicrometer-sized structural diameters. *Anal Chem* 67:4086–4090.
14. Kurulugama RT, et al. (2005) Scanning electrochemical microscopy of model neurons: Constant distance imaging. *Anal Chem* 77:1111–1117.
15. Takahashi Y, et al. (2011) Multifunctional nanoprobe for nanoscale chemical imaging and localized chemical delivery at surfaces and interfaces. *Angew Chem Int Ed Engl* 50:9638–9642.
16. Macpherson JV, Unwin PR (2000) Combined scanning electrochemical-atomic force microscopy. *Anal Chem* 72:276–285.
17. Hengstenberg A, Blochl A, Dietzel ID, Schuhmann W (2001) Spatially resolved detection of neurotransmitter secretion from individual cells by means of scanning electrochemical microscopy. *Angew Chem Int Ed Engl* 40:905–908.
18. Takahashi Y, Shiku H, Murata T, Yasukawa T, Matsue T (2009) Transfected single-cell imaging by scanning electrochemical optical microscopy with shear force feedback regulation. *Anal Chem* 81:9674–9681.
19. Schuhmann W, Nebel M, Eckhard K, Erichsen T, Schulte A (2010) 4D shearforce-based constant-distance mode scanning electrochemical microscopy. *Anal Chem* 82:7842–7848.
20. Osbourn DM, Sanger RH, Smith PJS (2005) Determination of single-cell oxygen consumption with impedance feedback for control of sample-probe separation. *Anal Chem* 77:6999–7004.
21. Ding ZF, Zhao XC, Diakowski PM (2010) Deconvoluting topography and spatial physiological activity of live macrophage cells by scanning electrochemical microscopy in constant-distance mode. *Anal Chem* 82:8371–8373.
22. Schuhmann W, Pahler M, Santana JJ, Souto RM (2011) Application of AC-SECM in corrosion science: Local visualization of inhibitor films on active metals for corrosion protection. *Chem Eur J* 17:905–911.
23. Fan FRF, Bard AJ (1999) Imaging of biological macromolecules on mica in humid air by scanning electrochemical microscopy. *Proc Natl Acad Sci USA* 96:14222–14227.
24. Comstock DJ, Elam JW, Pellin MJ, Hersam MC (2010) Integrated ultramicroelectrode-nanopipet probe for concurrent scanning electrochemical microscopy and scanning ion conductance microscopy. *Anal Chem* 82:1270–1276.
25. Williams CG, Edwards MA, Colley AL, Macpherson JV, Unwin PR (2009) Scanning micropipet contact method for high-resolution imaging of electrode surface redox activity. *Anal Chem* 81:2486–2495.
26. McKelvey K, Snowden ME, Peruffo M, Unwin PR (2011) Quantitative visualization of molecular transport through porous membranes: Enhanced resolution and contrast using intermittent contact-scanning electrochemical microscopy. *Anal Chem* 83:6447–6454.
27. Ebejer N, Schnippering M, Colburn AW, Edwards MA, Unwin PR (2010) Localized high resolution electrochemistry and multifunctional imaging: Scanning electrochemical cell microscopy. *Anal Chem* 82:9141–9145.
28. Bard AJ, Faulkner LR (2001) *Electrochemical Methods: Fundamentals and Applications*, (Wiley, New York), 2nd Ed, 26, pp 580–631.
29. Dumitrescu I, Unwin PR, Wilson NR, Macpherson JV (2008) Single-walled carbon nanotube network ultramicroelectrodes. *Anal Chem* 80:3598–3605.
30. Shao YH, Mirkin MV (1998) Probing ion transfer at the liquid/liquid interface by scanning electrochemical microscopy (SECM). *J Phys Chem B* 102:9915–9921.
31. Amplett JL, Denuault G (1998) Scanning electrochemical microscopy (SECM): An investigation of the effects of tip geometry on amperometric tip response. *J Phys Chem B* 102:9946–9951.
32. Lefrou C, Cornut R (2010) Analytical expressions for quantitative scanning electrochemical microscopy (SECM). *ChemPhysChem* 11:547–556.
33. Liebetrau JM, Miller HM, Baur JE (2003) Scanning electrochemical microscopy of model neurons: Imaging and real-time detection of morphological changes. *Anal Chem* 75:563–571.
34. Shevchuk AI, et al. (2006) Imaging proteins in membranes of living cells by high-resolution scanning ion conductance microscopy. *Angew Chem Int Ed Engl* 45:2212–2216.
35. Schulte A, Schuhmann W (2007) Single-cell microelectrochemistry. *Angew Chem Int Ed Engl* 46:8760–8777.
36. Novak P, et al. (2009) Nanoscale live-cell imaging using hopping probe ion conductance microscopy. *Nat Methods* 6:279–281.
37. Gonsalves M, et al. (2000) Scanning electrochemical microscopy as a local probe of oxygen permeability in cartilage. *Biophys J* 78:1578–1588.
38. Ciardiello F, Tortora G (2001) A novel approach in the treatment of cancer: Targeting the epidermal growth factor receptor. *Clin Cancer Res* 7:2958–2970.
39. Takahashi Y, et al. (2011) Electrochemical detection of receptor-mediated endocytosis by scanning electrochemical microscopy. *Phys Chem Chem Phys* 13:16569–16573.
40. Takahashi Y, et al. (2009) Electrochemical detection of epidermal growth factor receptors on a single living cell surface by scanning electrochemical microscopy. *Anal Chem* 81:2785–2790.
41. Shevchuk AI, et al. (2008) Imaging single virus particles on the surface of cell membranes by high-resolution scanning surface confocal microscopy. *Biophys J* 94:4089–4094.
42. Gorelik J, et al. (2002) Scanning surface confocal microscopy for simultaneous topographical and fluorescence imaging: Application to single virus-like particle entry into a cell. *Proc Natl Acad Sci USA* 99:16018–16023.
43. Isik S, Schuhmann W (2006) Detection of nitric oxide release from single cells by using constant-distance-mode scanning electrochemical microscopy. *Angew Chem Int Ed Engl* 45:7451–7454.
44. Sombers LA, et al. (2004) *J Neurosci* 24:303–309.
45. Bauermann LP, Schuhmann W, Schulte A (2004) An advanced biological scanning electrochemical microscope (Bio-SECM) for studying individual living cells. *Phys Chem Chem Phys* 6:4003–4008.
46. Robinson DL, Hermans A, Seipel AT, Wightman RM (2008) Monitoring rapid chemical communication in the brain. *Chem Rev* 108:2554–2584.
47. Lin YQ, Trouillon R, Safina G, Ewing AG (2011) Chemical analysis of single cells. *Anal Chem* 83:4369–4392.
48. Amatore C, Arbault S, Guille M, Lemaitre F (2008) Electrochemical monitoring of single cell secretion: Vesicular exocytosis and oxidative stress. *Chem Rev* 108:2585–2621.
49. Schroeder TJ, Jankowski JA, Senyshyn J, Holz RW, Wightman RM (1994) Zones of exocytotic release on bovine adrenal-medullary cells in culture. *J Biol Chem* 269:17215–17220.
50. Gorelik J, et al. (2006) A novel Z-groove index characterizing myocardial surface structure. *Cardiovasc Res* 72:422–429.